

Extremely small thermal conductivity of the Al-based Mackay-type 1/1-cubic approximants

Tsunehiro Takeuchi

*EcoTopia Science Institute, Nagoya University, Nagoya 464-8603, Japan
and Department of Crystalline Materials Science, Nagoya University, Nagoya 464-8603, Japan*

Naoyuki Nagasako and Ryoji Asahi

Toyota Central R&D Laboratories, Inc., Nagakute, Aichi 480-1192, Japan

Uichiro Mizutani

Toyota Physical & Chemical Research Institute, Nagakute, Aichi 480-1192, Japan

(Received 13 May 2006; published 10 August 2006)

Thermal conductivity (κ) of the Al-based Mackay-type 1/1-cubic approximants (α -phase) was investigated over a wide temperature range from 2 K to 300 K. Behaviors of $\kappa(T)$ observed for these 1/1-cubic approximants were essentially the same with those reported for the corresponding icosahedral quasicrystals; very small magnitude lower than 4.5 W/m K, small contribution of electrons, and possession of a local maximum and a local minimum around 30–50 K and 100–200 K, respectively. By analyzing measured lattice thermal conductivity $\kappa_{\text{lat}}(T)$ in terms both of local atomic arrangements and phonon dispersions, we revealed that $\kappa_{\text{lat}}(T)$ is greatly reduced by combination of the small group velocity of phonons and the enhanced umklapp process of phonon scattering. Those characteristics are brought about by the large lattice constant and vacancies in the structure.

DOI: [10.1103/PhysRevB.74.054206](https://doi.org/10.1103/PhysRevB.74.054206)

PACS number(s): 65.40.-b, 72.15.Eb, 63.20.Dj

I. INTRODUCTION

Icosahedral quasicrystals are widely known to possess a low thermal conductivity as low as ~ 1 W/m K (Ref. 1–5) and a large thermoelectric power up to $\sim 100\mu$ V/K.^{6–9} Those conditions together with the low electrical resistivity are necessities for the thermoelectric materials. The icosahedral quasicrystals, therefore, are regarded as one of the most plausible candidates for the practical thermoelectric materials. To utilize the icosahedral quasicrystals in thermoelectric devices, it is of great importance to investigate the mechanism leading to the small thermal conductivity. However, in spite of a large number of investigations,^{1–5,10,11} commonly acceptable scenario for the small thermal conductivity of the quasicrystals have not been established yet most likely because the quasiperiodicity inherent to quasicrystals prevented us from quantitatively investigating their atomic structure and its contribution to the low thermal conductivity.

The use of crystalline approximants as substitutes for the quasicrystals allows us to gain deep insight into the nature of quasicrystals because approximants possess the same local atomic arrangements as those in the quasicrystals, and furthermore, the structure analyses and band calculations which are hardly applicable for quasicrystals can be applied for the approximants. By comparing the measured physical properties between the quasicrystals and the approximants, one can separate the contribution of the local atomic arrangements from those of the long-range ordering (quasiperiodicity or periodicity), i.e., if the quasicrystals and their corresponding approximants possess a different or similar property, that property is brought about by the long-range ordering or local atomic arrangements, respectively. If one finds a property commonly observable in both phases, the dominant factors for it would be clearly investigated from the structure analysis and the band calculation of the approximants. Indeed, by

using the approximants of the icosahedral quasicrystals, we succeeded in revealing the mechanism leading to the large thermoelectric power and large electrical resistivity not only of the approximants but also of the corresponding icosahedral quasicrystals.^{9,12,13}

In order to investigate the origin of the low thermal conductivity observed for the Al-based Mackay-type icosahedral quasicrystals, we employed, in this study, their corresponding 1/1-cubic approximants. Those approximants are classified into the group of the α -phase originally found in the Al-Mn-Si alloy system.¹⁴ We performed the synchrotron radiation Rietveld analysis and a first principle calculation of the phonon dispersion on the basis of the refined structure parameters. The mechanism leading to the considerable reduction in the thermal conductivity were discussed in terms of the local atomic arrangements and phonon dispersion thus obtained. The contribution of quasiperiodicity to the small thermal conductivity is also discussed by comparing the measured thermal conductivity of the approximants with previously reported ones of the quasicrystals.

We demonstrate in this paper that the factors for the small thermal conductivity of the quasicrystals can be clearly revealed by the analyses on local atomic arrangements and phonon dispersions of the approximants. In addition, the results obtained by the present study of the approximants provides us useful information about the thermal conductivity not only of the approximants and quasicrystals but also of many other materials.

II. EXPERIMENTAL PROCEDURE

Mother ingots of the $\text{Al}_{82.6-x}\text{Re}_{17.4}\text{Si}_x$ ($x=7, 8, 9, 10$), $\text{Al}_{82.6-x}\text{Mn}_{17.4}\text{Si}_x$ ($x=8, 9, 11$), $\text{Al}_{76-x}\text{Cu}_7\text{Fe}_{17}\text{Si}_x$ ($x=9, 10, 11$), and $\text{Al}_{73.6}\text{Mn}_{17.4-y}\text{Fe}_y\text{Si}_9$ ($y=0, 5.5, 12.5$)

1/1-cubic approximants were prepared from pure elements, Al (purity 99.99%), Mn (99.95%), Fe (99.95%), Cu (99.99%), Re (99.99%), and Si (99.999%) using the arc-melting and the induction-melting techniques. Details of the sample preparation were reported elsewhere.^{12,13,16–18} The prepared ingots were cut into a rectangular shape of typically $\sim 1 \times 1 \times 10$ mm in dimension. These ingots were heat treated at 750 °C for 24 hours to improve the structure quality by removing the strain and voids introduced during the sample preparation. The phases in these samples were determined by the step-scanned powder x-ray diffraction measurements with a conventional Cu $K\alpha$ radiation. All samples were consisting solely of the 1/1-cubic approximant without possessing any precipitation of secondary phases. Ribbon samples were also prepared by the melt-spun technique for the measurements of electrical resistivity and powder x-ray diffraction of the Rietveld analysis. We used a copper wheel rotating at ~ 3000 rpm in a pressurized Ar atmosphere for the melt-spun operation.

The Rietveld analysis was performed on the synchrotron radiation powder diffraction spectra accumulated at the beam-line BL02B2 in SPring-8, Hyogo, Japan. A wavelength of $\lambda = 0.5\text{--}0.7$ Å, quartz glass capillary tubes of 0.2 mm in diameter, and imaging plates as the detector were employed with the low temperature (90 K) nitrogen gas blowing on the capillary tube containing the samples. The program RIETAN2000 developed by Izumi¹⁹ were used for the Rietveld analyses.

Electrical resistivity and thermal conductivity of these 1/1-cubic approximants were measured at the temperature range from 2 to 300 K using the Thermal Transport Option of the Physical Properties Measurement System (TTO-PPMS9), Quantum Design Inc. Four probes were placed on the samples; two of them were used to measure the temperature and the others were used to produce a constant heat flow along the samples. Some of the samples, especially the $\text{Al}_{73.6}\text{Mn}_{17.4-y}\text{Fe}_y\text{Si}_9$ with large y , had voids even after the heat treatments. The unfavorable effects of the voids on the thermoelectric properties were removed by estimating the reduction of the mean cross section of the bulk samples, that was calculated from the ratio of the measured density to the theoretical one. Specific heat was also measured for the $\text{Al}_{73.6}\text{Re}_{17.4}\text{Si}_9$ 1/1-cubic approximants over the temperature range from 2 to 300 K with the PPMS9.

Lattice thermal conductivity $\kappa_{\text{lat}}(T)$ was roughly estimated from the observed thermal conductivity $\kappa_{\text{obs}}(T)$ by subtracting the electron thermal conductivity $\kappa_{\text{el}}(T)$ that was calculated from the electrical resistivity $\rho(T)$ using the Wiedemann-Franz law, $\kappa_{\text{el}}(T) = \sigma(T)LT$, where $\sigma(T) = 1/\rho(T)$ and L represent electrical conductivity and the Lorenz number, respectively.

Phonon dispersion was calculated on the $\text{Al}_{73.6}\text{Re}_{17.4}\text{Si}_9$ 1/1-cubic approximant of the disordering-free structure.^{12,18} Starting from the most reliable structure parameters determined by the synchrotron radiation Rietveld analysis, we calculated total energy and atomic force by the projector augmented wave method as implemented in VASP code,²⁰ which enabled us to obtain the phonon dispersion by the direct method.²¹ The integration in the k space for the electronic

structure calculations was performed with the Methfessel-Paxton special k points of $2 \times 2 \times 2$ meshes. The dynamical matrix in the direct method was calculated employing atomic displacements of ± 0.03 Å. The phonon density of states were calculated with the 2000 Monte Carlo sampling k points. The lattice specific heats are estimated from the total phonon DOS based on the quasiharmonic approximation.

III. RESULTS

A. Structure of the approximants

All 1/1-cubic approximants employed in this study are classified into the group of the α -phase originally found in the Al-Mn-Si alloy system.^{14–17} The structure of these approximants is characterized by the large lattice constant of $a = 12\text{--}13$ Å with the Mackay clusters of 54 atoms in the center and vertices of the unit cell.²² The Mackay cluster possesses the icosahedral symmetry ($m\bar{3}5$), but the symmetry of the cubic approximants is reduced into $m\bar{3}$ because the “glue” sites, which connect the Mackay clusters, destroy the icosahedral symmetry (the fivefold symmetry).

The ordering of the glue sites leads to the different type of symmetries; the $\text{Al}_{82.6-x}\text{Re}_{17.4}\text{Si}_x$ and $\text{Al}_{82.6-x}\text{Mn}_{17.4}\text{Si}_x$ 1/1-cubic approximants possess the $Pm\bar{3}$ symmetry,^{9,13} while the $\text{Al}_{76-x}\text{Cu}_7\text{Fe}_{17}\text{Si}_x$ approximants are classified into the group of the $Im\bar{3}$ symmetry. The $\text{Al}_{73.6}\text{Mn}_{17.4-y}\text{Fe}_y\text{Si}_9$ 1/1-cubic approximants possessing the $Pm\bar{3}$ symmetry at small Fe concentrations turn up to have the $Im\bar{3}$ symmetry at high Fe concentrations of $y > 5$ at.%.¹⁶ The $Im\bar{3}$ -type 1/1 approximants have 36 positions in the glue sites. On the other hand, the $Pm\bar{3}$ ordering of the glue sites reduces the number of atomic positions into 30. Hence the cubic unit cell of the 1/1-cubic approximants is build up with 138–144 ($= 54 \times 2 + 30 - 36$) atoms.

The local atomic arrangements of the $\text{Al}_{82.6-x}\text{Re}_{17.4}\text{Si}_x$ and $\text{Al}_{73.6}\text{Mn}_{17.4-y}\text{Fe}_y\text{Si}_9$ 1/1-cubic approximants refined by the the synchrotron radiation Rietveld analyses were already reported in our previous papers.^{12,16} In this study, we analyzed the two other series of the approximants; $\text{Al}_{76-x}\text{Cu}_7\text{Fe}_{17}\text{Si}_x$ ($x = 9, 10, 11$) and $\text{Al}_{82.6-x}\text{Mn}_{17.4}\text{Si}_x$ ($x = 7, 9, 11$). Reliability of the present analyses was confirmed by the satisfactory reduced reliable factors (R -factors) (Ref. 23) and the resulting compositions well representing the nominal ones. The calculated spectra of the typical examples are shown in Figs. 1(b) and 1(c) together with the measured ones, and the refined structure parameters and the R -factors are summarized in Tables I and II.

We found, as a consequence of the Rietveld analyses, that the number of vacancies in the glue sites (N_{vac}) varies with composition regardless of the alloy systems. The determined N_{vac} are summarized in Table III. The mechanism producing these vacancies has been already discussed in our previous papers in terms of the electron concentration.¹⁶ Instead of explaining it in detail, we stress here that the presence of the vacancies in the glue sites strongly affects the lattice thermal conductivity κ_{lat} as shown in the following section.

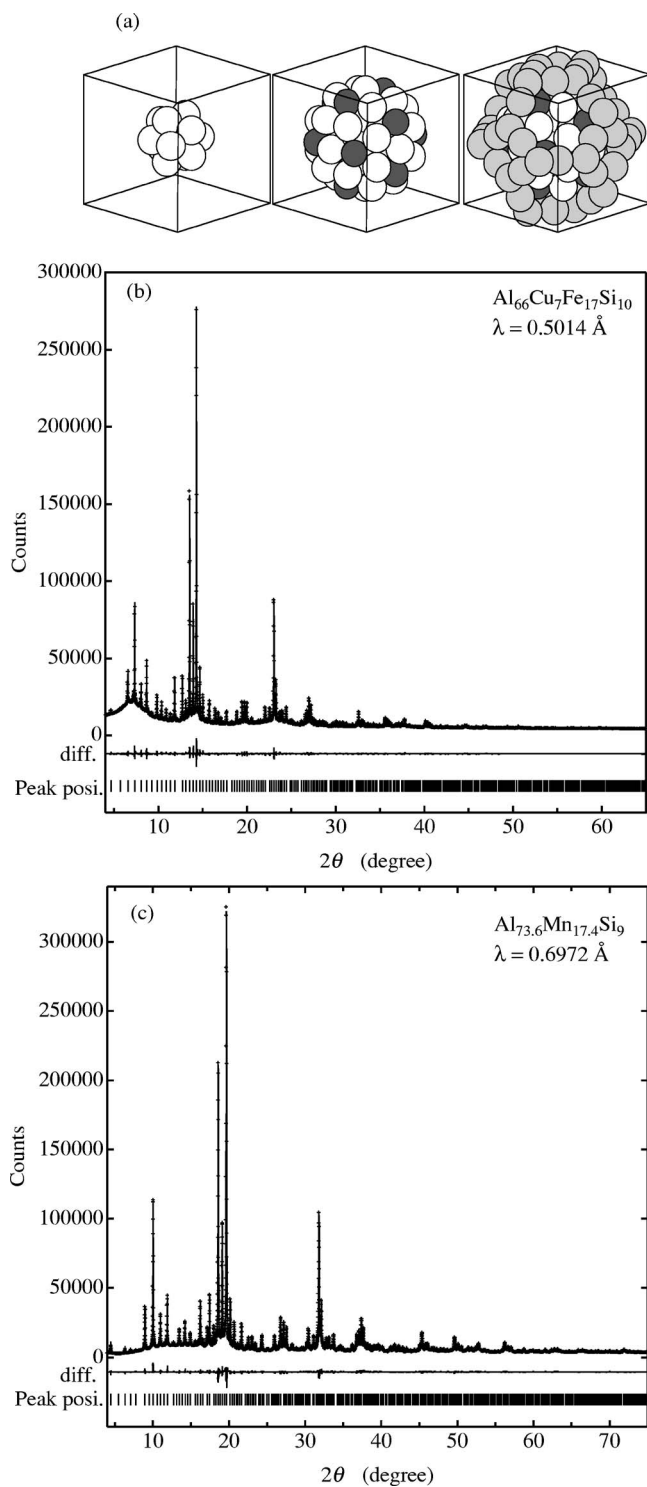


FIG. 1. (a) Structure of the Mackay-type 1/1-cubic approximants. The white and dark gray circles represent sites mainly occupied by Al and the half-filled transition metal elements (Fe, Mn, Re), respectively. The glue sites are shown with the light gray circles. The x-ray diffraction spectra calculated by the Rietveld analysis are superimposed on the measured ones for (b) $\text{Al}_{66}\text{Cu}_7\text{Fe}_{17}\text{Si}_{10}$ and (c) $\text{Al}_{73.6}\text{Mn}_{17.4}\text{Si}_9$. Peak positions and the difference spectra are also shown at the bottom of each panel.

B. Observed thermal conductivity

Figures 2(a1)–2(a4) show the temperature dependence of the thermal conductivity $\kappa_{\text{obs}}(T)$ of the 1/1-cubic approximants. All samples possess very small $\kappa_{\text{obs}}(T)$ less than 4.5 W/m K over the whole temperature range of the measurement. The magnitude of $\kappa_{\text{obs}}(T)$ of the $\text{Al}_{82.6-x}\text{Re}_{17.4}\text{Si}_x$, the $\text{Al}_{71.6}\text{Mn}_{17.4}\text{Si}_{11}$, and the $\text{Al}_{73.6}\text{Mn}_{4.9}\text{Fe}_{12.5}\text{Si}_9$ are especially small, possessing less than 2 W/m K. These small values of $\kappa_{\text{obs}}(T)$ are comparable with those reported for the Al-based icosahedral quasicrystals.^{1–3} It is suggested, therefore, that the quasiperiodicity specific only to the quasicrystals does not play a crucially important role in reducing the thermal conductivity.

One may also realize that $\kappa_{\text{obs}}(T)$ of the $\text{Al}_{82.6-x}\text{Re}_{17.4}\text{Si}_x$ possesses, on the whole, smaller magnitude than that of the other approximants. Since the Re atom has the heaviest atomic weight among all constituent elements, it is naturally considered that the κ of the approximants is effectively reduced by the presence of a heavy constituent element. The role of the heavy elements in reducing the magnitude of $\kappa(T)$ will be discussed in detail in Sec. IV.

Generally speaking, heats in the solids are conducted by electrons and lattice. Since the electron contribution to the thermal conductivity [$\kappa_{\text{el}}(T)$] can be roughly estimated from the electrical resistivity $\rho(T)$ using the well-known Wiedemann-Franz law, the thermal conductivity due to the lattice $\kappa_{\text{lat}}(T)$ was estimated by subtracting $\kappa_{\text{el}}(T)$ from $\kappa_{\text{obs}}(T)$. The calculated $\kappa_{\text{el}}(T)$ of the present 1/1-cubic approximants was superimposed on $\kappa_{\text{obs}}(T)$ in Figs. 2(a1)–2(a4). The deduced lattice thermal conductivity $\kappa_{\text{lat}}(T)$ and the electrical resistivity $\rho(T)$ were also shown in Figs. 2(b1)–2(b4) and 2(c1)–2(c4), respectively. The large magnitude of the electrical resistivity exceeding 800 $\mu\Omega$ cm provides rather small $\kappa_{\text{el}}(T)$ less than 1 W/m K even at room temperature. It can be safely argued, therefore, that the characteristic behaviors in the thermal conductivity observed for the approximants are mainly brought about by the lattice rather than by electrons.

With increasing temperature from 2 K, $\kappa_{\text{lat}}(T)$ of the approximants increases and then starts to decrease after becoming maximal at $T_{\text{peak}}=40\text{--}50$ K. With further increasing temperature, $\kappa_{\text{lat}}(T)$ possesses almost no temperature dependence regardless of the sample compositions. The moderately increasing tendency observed in $\kappa_{\text{obs}}(T)$ at high temperatures above 150 K is almost disappeared in $\kappa_{\text{lat}}(T)$. The increasing tendency in $\kappa_{\text{obs}}(T)$ of the approximants above 150 K is mainly caused by the temperature dependence of κ_{el} . The drastic increase of the $\kappa_{\text{lat}}(T)$ at high temperatures above 200 K reported for some icosahedral quasicrystals² was not observed for the present approximants at least in the measured temperature range. Increasing tendency of $\kappa_{\text{lat}}(T)$ of the quasicrystals at high temperature might be related to the increasing C above $3R$ with increasing temperature reported by Edagawa *et al.*²⁴ The lack of the quasiperiodicity could be the reason for the almost constant κ_{lat} of the approximants at high temperature.

In Figs. 3(a)–3(d), the lattice thermal conductivity at T_{peak} and 300 K is plotted as a function of composition. A strong

TABLE I. Results of the Rietveld refinement of the $\text{Al}_{82.6-x}\text{Mn}_{17.4}\text{Si}_x$ 1/1-1/1-1/1 approximants ($x=7, 9, 12$).

(a) $\text{Al}_{75.6}\text{Mn}_{17.4}\text{Si}_7$, resulting composition $\text{Al}_{74.0}\text{Mn}_{17.6}\text{Si}_{8.4}$ $R_{\text{wp}}=2.54\%$, $R_e=1.09\%$, $R_I=1.07\%$, $R_F=0.63\%$ $Pm\bar{3}$, $a=12.6131(1)$ Å, $B_{\text{iso}}=0.393(3)$ (Å ²)						
Cluster	Site	Atoms	occ.	x	y	z
Inner	IIa(12j)	Al	1.00	0.1677(2)	0.1012(2)	0.0000
Ico.	IIb(12k)	Al	1.00	0.3359(2)	0.3985(2)	0.5000
Mackay	MI1a(6e)	Al	1.00	0.3617(3)	0.0000	0.0000
Ico.	MI1b(6h)	Al	1.00	0.1189(3)	0.5000	0.5000
	MI2a(24l)	Al	1.00	0.1182(1)	0.1864(2)	0.2987(2)
	MI2b(24l)	Al	1.00	0.3889(1)	0.3140(2)	0.1958(2)
	TMa(12j)	Mn	1.00	0.3272(1)	0.2000(1)	0.0000
	TMb(12k)	Mn	1.00	0.1800(1)	0.3037(1)	0.5000
Glue	G1(12k)	Al	0.942(4)	0.1285(2)	0.1139(2)	0.5000
	G2(12j)	Si	0.961(4)	0.3280(2)	0.4025(2)	0.0000
	G3(6f)	Al	0.957(4)	0.2944(3)	0.0000	0.5000
(b) $\text{Al}_{73.6}\text{Mn}_{17.4}\text{Si}_9$, resulting composition $\text{Al}_{73.3}\text{Mn}_{17.6}\text{Si}_{9.1}$ $R_{\text{wp}}=2.76\%$, $R_e=1.12\%$, $R_I=1.26\%$, $R_F=0.81\%$ $Pm\bar{3}$, $a=12.5975(1)$ Å, $B_{\text{iso}}=0.338(3)$ (Å ²)						
Inner	IIa(12j)	Al	1.00	0.1667(2)	0.1010(2)	0.0000
Ico.	IIb(12k)	Al	1.00	0.3355(2)	0.3996(2)	0.5000
Mackay	MI1a(6e)	Al	1.00	0.3637(3)	0.0000	0.0000
Ico.	MI1b(6h)	Al	1.00	0.1211(3)	0.5000	0.5000
	MI2a(24l)	Al	1.00	0.1177(1)	0.1871(2)	0.2982(2)
	MI2b(24l)	Al	1.00	0.3901(1)	0.3137(2)	0.1964(2)
	TMa(12j)	Mn	1.00	0.3280(1)	0.1995(1)	0.0000
	TMb(12k)	Mn	1.00	0.1798(1)	0.3058(1)	0.5000
Glue	G1(12k)	Al	0.946(4)	0.1221(2)	0.1154(2)	0.5000
	G2(12j)	Si	0.934(4)	0.3295(2)	0.4022(2)	0.0000
	G3(6f)	Al	0.8(2)	0.291(8)	0.0000	0.5000
	G3'(6f)	Si	0.2(2)	0.292(9)	0.0000	0.5000
(c) $\text{Al}_{70.6}\text{Mn}_{17.4}\text{Si}_{12}$, resulting composition $\text{Al}_{70.1}\text{Mn}_{17.6}\text{Si}_{12.3}$ $R_{\text{wp}}=2.30\%$, $R_e=1.10\%$, $R_I=1.43\%$, $R_F=0.70\%$ $Pm\bar{3}$, $a=12.5630(1)$ Å, $B_{\text{iso}}=0.346(4)$ (Å ²)						
Inner	IIa(12j)	Al	1.00	0.1657(3)	0.1009(2)	0.0000
Ico.	IIb(12k)	Al	1.00	0.3368(3)	0.4000(3)	0.5000
Mackay	MI1a(6e)	Al	1.00	0.3645(4)	0.0000	0.0000
Ico.	MI1b(6h)	Al	1.00	0.1242(4)	0.5000	0.5000
	MI2a(24l)	Al	1.00	0.1182(1)	0.1887(2)	0.2976(2)
	MI2b(24l)	Al	1.00	0.3914(2)	0.3134(2)	0.1957(2)
	TMa(12j)	Mn	1.00	0.3273(1)	0.1983(1)	0.0000
	TMb(12k)	Mn	1.00	0.1797(1)	0.3082(1)	0.5000
Glue	G1(12k)	Al	0.948(5)	0.1241(2)	0.1170(2)	0.5000
	G2(12j)	Si	0.918(4)	0.3307(2)	0.4019(2)	0.0000
	G3(6f)	Si	0.96(2)	0.289(1)	0.0000	0.5000

TABLE II. Results of the Rietveld refinement of the $\text{Al}_{86-x}\text{Cu}_7\text{Fe}_{17}\text{Si}_x$ 1/1-1/1-1/1 approximants ($x=9, 10, 11$).

(a) $\text{Al}_{67}\text{Cu}_7\text{Fe}_{17}\text{Si}_9$, resulting composition $\text{Al}_{65.9}\text{Cu}_{7.5}\text{Fe}_{17.0}\text{Si}_{9.6}$ $R_{\text{wp}}=1.36\%$, $R_e=1.09\%$, $R_I=1.49\%$, $R_F=2.28\%$ $Im\bar{3}$, $a=12.4614(1)$ Å, $B_{\text{iso}}=0.579(7)$ (Å ²)						
Cluster	Site	Atoms	occ.	x	y	z
Inner	II(24g)	Al	0.837(4)	0.1662(9)	0.1000(9)	0.0000
Ico.	II'(24g)	Cu	0.163(4)	0.162(2)	0.103(2)	0.0000
Mackay	MI1(12d)	Al	0.903(5)	0.3710(4)	0.0000	0.0000
Ico.	MI1'(12d)	Cu	0.097(5)	0.389(1)	0.0000	0.0000
	MI2(48h)	Al	0.915(3)	0.1148(2)	0.1861(2)	0.3045(2)
	MI2'(48h)	Cu	0.085(3)	0.1167(8)	0.1806(8)	0.2792(7)
	TM(24g)	Fe	1.00	0.3216(1)	0.1981(1)	0.0000
Glue	G1(24g)	Si	0.569(6)	0.3680(3)	0.3889(3)	0.0000
	G1'(24g)	Al	0.384(6)	0.3158(6)	0.4062(4)	0.0000
	G1''(24g)	Cu	0.060(3)	0.356(1)	0.224(1)	0.0000
	G2(12e)	Al	0.727(5)	0.30885(3)	0.0000	0.5000
	G2'(12e)	Al	0.039(6)	0.23233(3)	0.0000	0.5000
(b) $\text{Al}_{66}\text{Cu}_7\text{Fe}_{17}\text{Si}_{10}$, resulting composition $\text{Al}_{65.2}\text{Cu}_{8.0}\text{Fe}_{17.0}\text{Si}_{9.8}$ $R_{\text{wp}}=1.88\%$, $R_e=1.07\%$, $R_I=1.25\%$, $R_F=1.78\%$ $Im\bar{3}$, $a=12.437(1)$ Å, $B_{\text{iso}}=0.546(8)$ (Å ²)						
Inner	II(24g)	Al	0.823(3)	0.1680(5)	0.0999(6)	0.0000
Ico.	II'(24g)	Cu	0.177(3)	0.158(1)	0.102(1)	0.0000
Mackay	MI1(12d)	Al	0.910(5)	0.3676(4)	0.0000	0.0000
Ico.	MI1'(12d)	Cu	0.090(5)	0.396(1)	0.0000	0.0000
	MI2(48h)	Al	0.901(2)	0.1146(2)	0.1833(2)	0.2961(2)
	MI2'(48h)	Cu	0.099(2)	0.1212(7)	0.1928(8)	0.3212(6)
	TM(24g)	Fe	1.00	0.3229(1)	0.1985(1)	0.0000
Glue	G1(24g)	Si	0.578(5)	0.3708(4)	0.3895(3)	0.0000
	G1'(24g)	Al	0.358(5)	0.3131(6)	0.4068(5)	0.0000
	G1''(24g)	Cu	0.048(2)	0.356(1)	0.252(2)	0.0000
	G2(12e)	Al	0.695(5)	0.3095(4)	0.0000	0.5000
	G2'(12e)	Al	0.108(5)	0.198(3)	0.0000	0.5000
(c) $\text{Al}_{65}\text{Cu}_7\text{Fe}_{17}\text{Si}_{11}$, resulting composition $\text{Al}_{64.5}\text{Cu}_{8.0}\text{Fe}_{17.1}\text{Si}_{10.4}$ $R_{\text{wp}}=2.09\%$, $R_e=1.03\%$, $R_I=1.42\%$, $R_F=1.60\%$ $Im\bar{3}$, $a=12.424(1)$ Å, $B_{\text{iso}}=0.441(7)$ (Å ²)						
Inner	II(24g)	Al	0.822(3)	0.1678(6)	0.0996(7)	0.0000
Ico.	II'(24g)	Cu	0.178(3)	0.159(1)	0.104(1)	0.0000
Mackay	MI1(12d)	Al	0.907(6)	0.3686(4)	0.0000	0.0000
Ico.	MI1'(12d)	Cu	0.093(5)	0.392(1)	0.0000	0.0000
	MI2(48h)	Al	0.899(3)	0.1148(2)	0.1835(3)	0.2960(2)
	MI2'(48h)	Cu	0.101(3)	0.1183(7)	0.1917(8)	0.3218(6)
	TM(24g)	Fe	1.0	0.3227(1)	0.1986(1)	0.0000
Glue	G1(24g)	Si	0.555(6)	0.3718(4)	0.3896(3)	0.0000
	G1'(24g)	Al	0.358(6)	0.3166(7)	0.4046(5)	0.0000
	G1''(24g)	Cu	0.045(3)	0.339(1)	0.248(2)	0.0000
	G2(12e)	Al	0.668(5)	0.3098(4)	0.0000	0.5000
	G2'(12e)	Si	0.100(5)	0.200(3)	0.0000	0.5000

TABLE III. Number of atoms in the unit cell of the 1/1-cubic approximants.

Composition	N_{total}	N_{vac}	References
$\text{Al}_{75.6}\text{Re}_{17.4}\text{Si}_7$	136.44	1.56	12
$\text{Al}_{73.6}\text{Re}_{17.4}\text{Si}_9$	138.00	0.00	12
$\text{Al}_{70.6}\text{Re}_{17.4}\text{Si}_{12}$	134.64	3.36	12
$\text{Al}_{75.6}\text{Mn}_{17.4}\text{Si}_7$	136.58	1.42	
$\text{Al}_{73.6}\text{Mn}_{17.4}\text{Si}_9$	136.57	1.43	
$\text{Al}_{70.6}\text{Mn}_{17.4}\text{Si}_{12}$	136.18	1.82	
$\text{Al}_{67}\text{Cu}_7\text{Fe}_{17}\text{Si}_9$	141.49	2.51	
$\text{Al}_{66}\text{Cu}_7\text{Fe}_{17}\text{Si}_{10}$	141.26	2.74	
$\text{Al}_{65}\text{Cu}_7\text{Fe}_{17}\text{Si}_{11}$	140.21	3.79	
$\text{Al}_{73.6}\text{Mn}_{12.4}\text{Fe}_5\text{Si}_9$	135.72	2.28	16
$\text{Al}_{73.5}\text{Mn}_{11.3}\text{Fe}_{6.2}\text{Si}_9^{\text{a}}$	134.06	3.94	16

^aAlthough the symmetry of the $\text{Al}_{73.5}\text{Mn}_{11.3}\text{Fe}_{6.2}\text{Si}_9$ is $Im\bar{3}$, the number of vacancies in it was calculated by $N_{\text{vac}} = 138 - N_{\text{total}}$ as that in the $Pm\bar{3}$ type $\text{Al}_{73.6}\text{Mn}_{12.4}\text{Fe}_5\text{Si}_9$.

composition dependence was clearly observed in both $\kappa_{\text{lat}}(T_{\text{peak}})$ and $\kappa_{\text{lat}}(300 \text{ K})$. By taking a careful look on the $\kappa_{\text{lat}}(T)$ and the refined structure parameters, we realized that the magnitude of $\kappa_{\text{lat}}(T)$ has a close relation with the number of vacancies in the glue sites (N_{vac}). The lattice thermal conductivity at T_{peak} and 300 K are plotted in Fig. 3(e) as a function of N_{vac} . Obviously both $\kappa_{\text{lat}}(T_{\text{peak}})$ and $\kappa_{\text{lat}}(300 \text{ K})$ decrease with increasing N_{vac} . This result seemingly sounds natural, because κ_{lat} below 300 K is dominated by phonon conduction and point defects generally scatter the phonons to

reduce the mean free path. Thus κ_{lat} could become small simply by the reduction in the mean free path of phonons with increasing N_{vac} . However, quantitative analysis on the $\kappa_{\text{lat}}(T)$ revealed that N_{vac} affects $\kappa_{\text{lat}}(T)$ not only by shortening the mean free path of phonons but also by some additional effects, which will be discussed in detail later.

If phonons are well defined as a collective excitation, lattice thermal conductivity in an isotropic system, such as icosahedral quasicrystals and their approximants, can be roughly estimated by using the equation

$$\kappa = (1/3)Cv_{\text{ave}}\lambda, \quad (1)$$

where C , v_{ave} , and λ represent specific heat, mean group velocity, and mean free path of phonons, respectively.²⁵ The total momentum of phonons is not strongly altered by the normal process but mainly by the umklapp process. Therefore the umklapp process of the phonon scattering rather than the normal process should be taken into account to estimate λ of phonons in Eq. (1).

The local maximum in κ_{lat} at T_{peak} , which is generally observed for crystalline materials, indicates that λ of phonons increases with decreasing temperature at $T > T_{\text{peak}}$ as the probability of the umklapp process decreases. With further decreasing the temperature below T_{peak} , the increase of λ is significantly suppressed because it is limited by the macroscopic size factors, such as sample dimension, grain size, mean distances of the dislocations, etc. At this temperature range, the mean group velocity of phonons generally remains constant at the sound velocity v_s because of absence of optical phonons. Almost temperature independent λ , the constant v_{ave} , and the rapidly decreasing specific heat C with decreasing temperature cause the drastic reduction in $\kappa_{\text{lat}}(T)$ below T_{peak} . These behaviors described above were certainly

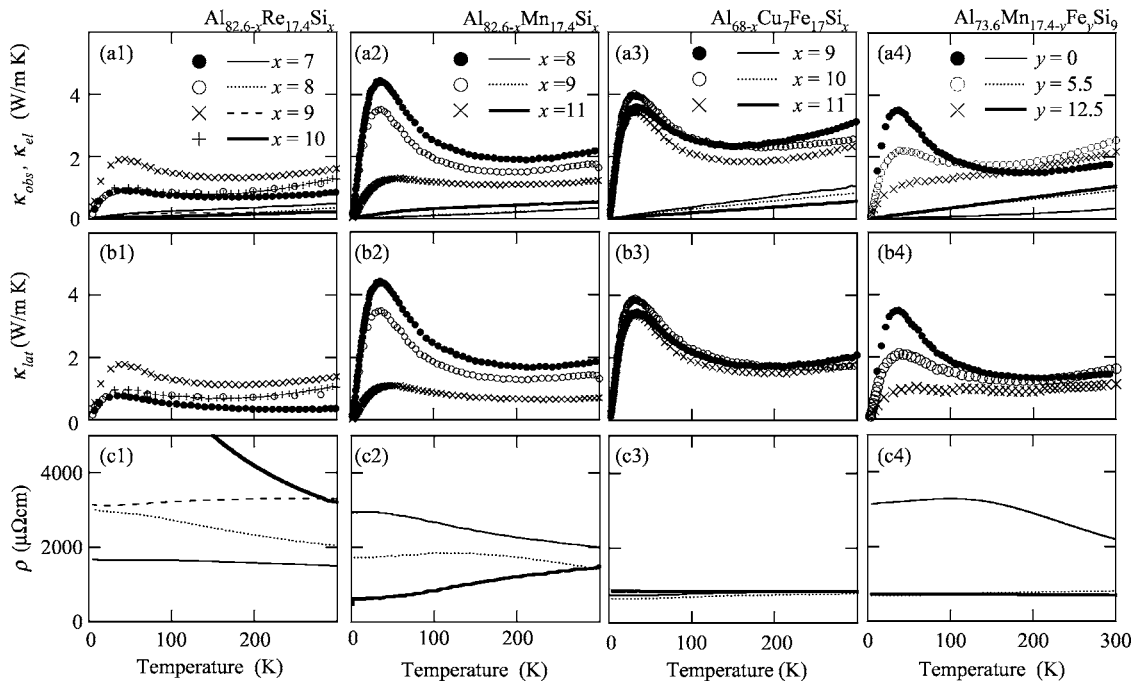


FIG. 2. (a1)–(a4) Measured thermal conductivity (markers) and electron thermal conductivity (lines), (b1)–(b4) the lattice thermal conductivity, and (c1)–(c4) the electrical resistivity of the 1/1-cubic approximants.

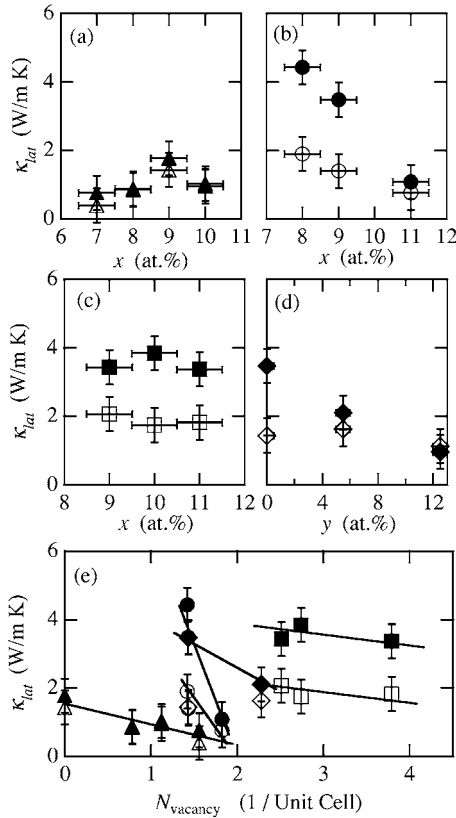


FIG. 3. Lattice thermal conductivity of the (a) $\text{Al}_{82.6-x}\text{Re}_{17.4}\text{Si}_9$, (b) $\text{Al}_{82.6-x}\text{Mn}_{17.4}\text{Si}_9$, (c) $\text{Al}_{76-x}\text{Cu}_7\text{Fe}_{17}\text{Si}_9$, and (d) $\text{Al}_{73.6}\text{Mn}_{17.4-y}\text{Fe}_9\text{Si}_9$ 1/1-cubic approximants. The data at room temperature and the peak temperature, $\kappa_{\text{lat}}(300\text{K})$ and $\kappa_{\text{lat}}(T_{\text{peak}})$, are shown with the open markers and the solid markers, respectively. (e) $\kappa_{\text{lat}}(300\text{K})$ and $\kappa_{\text{lat}}(T_{\text{peak}})$ as a function of number of vacancies in the lattice N_{vac} . N_{vac} of the samples that have no refined structure parameters were estimated from the interpolation of the available data shown in Table III. The same markers as those in (a)–(d) are used in (e). Obviously, both $\kappa_{\text{lat}}(300\text{K})$ and $\kappa_{\text{lat}}(T_{\text{peak}})$ decreases with increasing N_{vac} both at room temperature and the peak temperature.

observed for the present approximants and also reported for the corresponding quasicrystals.^{1–4} It is safely argued, therefore, that phonons are well defined as a collective mode in the present approximants, and perhaps in the corresponding quasicrystals.

We roughly estimated λ at T_{peak} in the $\text{Al}_{74.6}\text{Mn}_{17.4}\text{Si}_8$ by using the Debye model with the Debye temperature $\Theta_D \sim 560$ K determined by the low temperature specific heat measurement.¹³ The resulting λ was a few hundred Å, that is long enough to let us believe the presence of phonons in the approximants. In the corresponding quasicrystals, presence of the well-defined phonons was reported on the basis of the inelastic neutron and x-ray diffraction measurements.^{26–28} Theoretical calculations also predicted the presence of phonons as a collective mode in the quasicrystals.²⁹

The results obtained by the present experiments of the thermal conductivity suggest that the lattice thermal conductivity of the 1/1-cubic approximants and perhaps of their corresponding quasicrystals was dominated by phonons, and

that presence of vacancies reduces the magnitude of the thermal conductivity most likely by shortening λ of the phonons. Nevertheless, one may notice that this mechanism is not specific to the quasicrystals and approximants but applicable for many other solid materials. We must say, therefore, that the mechanism leading to the extremely small thermal conductivity of the icosahedral quasicrystals and their approximants has not been well revealed yet at this stage.

In addition, we found three experimental facts which are hard to understand. The first one beyond our comprehension is the strong composition dependence of $\kappa_{\text{lat}}(300\text{K})$. It is natural to consider that λ of phonons is saturated at high temperatures where the very weak temperature dependence of $\kappa_{\text{lat}}(T)$ is observed. If vacancies affect $\kappa_{\text{lat}}(T)$ by simply reducing λ of phonons, a less significant N_{vac} dependence in $\kappa_{\text{lat}}(T)$ is expected at high temperatures because of the saturated λ . However, at 300 K, the magnitude of $\kappa_{\text{lat}}(T)$ does decrease with increasing N_{vac} . The second fact is the presence of different slopes in the $\kappa_{\text{lat}}-N_{\text{vac}}$ plot shown in Fig. 3(e). It is expressed, in other words, that the observed $\kappa_{\text{lat}}(T)$ cannot be placed in order simply by the number of vacancies in the glue sites. The third fact is the observation of the small κ_{lat} for the disordering free sample, i.e., thermal conductivity of the $\text{Al}_{73.6}\text{Re}_{17.4}\text{Si}_9$ has small magnitude less than 2 W/m K even though it has no disordering nor vacancies in the structure.

In order to clarify the unraveled factors leading to the small thermal conductivity, we investigated the phonon dispersion using the first-principles calculations.

C. Phonon dispersion

Figures 4(a) and 4(b) show the phonon dispersion of the $\text{Al}_{73.6}\text{Re}_{17.4}\text{Si}_9$ 1/1-cubic approximant calculated with the Rietveld refined structure parameters.^{12,18} The lattice specific heat calculated from the phonon dispersion quantitatively reproduces the measured one in its magnitude and temperature dependence as shown in Fig. 4(c). This fact strongly indicates reliability of the present phonon calculation. The use of the disordering-free structure should be responsible for the reliable phonon dispersion.

The first Brillouin zone (FBZ) of the approximant has small volume in the reciprocal space because of their large lattice constant (12–13 Å). Three acoustic branches, one longitudinal and two transverse modes, are clearly observed at the lowest energy region [see Fig. 4(b)]. Those acoustic phonon branches are limited in very low energy range below 8 meV, and the optical phonon branches are densely generated above 10 meV. Excitation of the optical phonons is expected even at low temperature below 100 K.

The vibrational density of states $D(\varepsilon)$ calculated from the phonon dispersions are shown in Fig. 5(b) together with that calculated by the Debye model $D_D(\varepsilon)$ using the Debye temperature determined from the low temperature specific heat. $D_D(\varepsilon)$ overlaps with $D(\varepsilon)$ in a very narrow energy range below 8 meV, but starts to deviate from $D(\varepsilon)$ above 8 meV because of the densely lying optical phonon branches. The use of the Debye model is inappropriate even at low temperatures below 100 K for the present 1/1-cubic approxi-

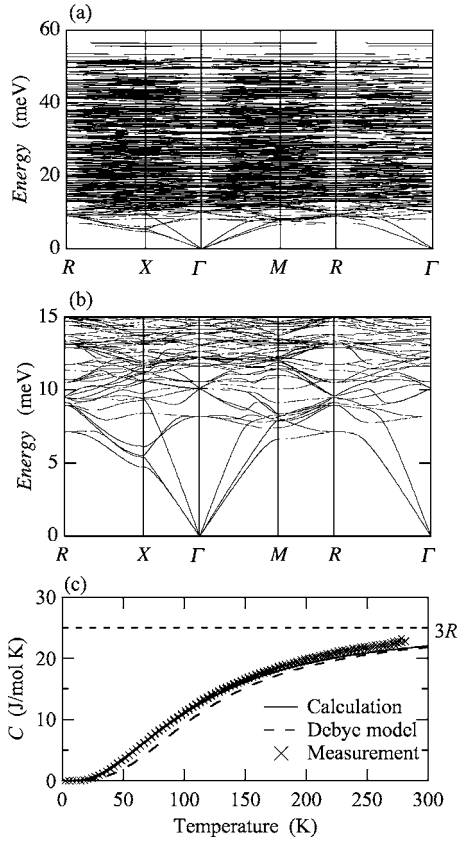


FIG. 4. (a) The calculated phonon dispersion of the $\text{Al}_{73.6}\text{Re}_{17.4}\text{Si}_9$ 1/1-cubic approximant. The calculated phonon dispersion at the low energy range below 15 meV is magnified in (b). (c) Specific heat C calculated from the phonon dispersion together with the measured C and that of the Debye model. The calculated C quantitatively reproduced the measured one, strongly indicating reliability of the calculated phonon dispersion. Only at high temperatures above 200 K, the lattice thermal expansion, which was not taken into account in the present calculation, causes the very minor deviation of the calculated C from the measured one.

nants. Inappropriate use of the Debye model even at low temperature was clearly confirmed by observing the product of $D(\varepsilon)$ and the Bose-Einstein distribution function $f_{\text{BE}}(\varepsilon, T)$ showing a large number of optical phonons excited even at low temperatures below 100 K [see $D(\varepsilon) \times f_{\text{BE}}(\varepsilon, 50 \text{ K})$ shown in Fig. 5(b)] Specific heat deduced from the Debye model obviously deviates from the measured one at temperatures above 30 K as shown in Fig. 4(c).

These characteristics in the phonon dispersion reduce the thermal conductivity in two different ways; (a) reducing the mean group velocity and (b) intensively activating umklapp scattering. The mean group velocity of the phonons is reduced by the excited optical phonons because optical phonons generally possess a much slower group velocity than the sound velocity v_s . In addition, umklapp processes are intensively generated even at low temperature because the small Brillouin zone allows the phonons to be excited near the zone boundary where the umklapp processes are easily generated. Notably, this mechanism well accounts for the small lattice thermal conductivity of the disordering-free $\text{Al}_{73.6}\text{Re}_{17.4}\text{Si}_9$ 1/1-cubic approximant.

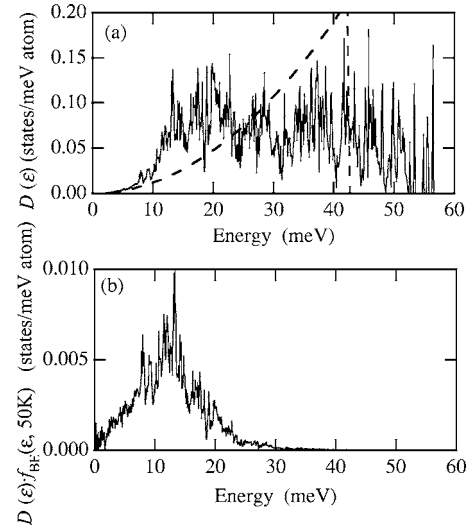


FIG. 5. (a) Vibrational density of states $[D(\varepsilon)]$ calculated for the $\text{Al}_{73.6}\text{Re}_{17.4}\text{Si}_9$ 1/1-cubic approximant. A large number of sharp peaks are generated by the optical phonon branches. The calculated $D(\varepsilon)$ fits the Debye model only in a very narrow energy range below 8 meV. (b) Product of the calculated $D(\varepsilon)$ and the Bose-Einstein distribution function $f_{\text{BE}}(\varepsilon, T)$ at 50 K. A large number of optical phonons are excited even at 50 K.

In the next section, by introducing a simple model of the phonon dispersion, we prove validity of the scenario described above and reveal the factors leading to the small lattice thermal conductivity of the approximants in more detail.

IV. DISCUSSIONS

A. Basic assumptions and formulations

Let us now consider a hypothetical system of a cubic unit cell with a lattice constant a and N atoms in it. The number of atoms in the unit cell N increases in roughly proportion to a^3 , provided that the density is kept almost constant. Three acoustic branches and $3N-3$ optical phonon branches are generated in FBZ. In the vibrational density of states $D(\varepsilon)$, one should find $3N-3$ sharp peaks from the optical phonon branches together with a parabolic portion of the acoustic branches at the lowest energy range. We assume here that the $N-1$ sharp peaks are uniformly distributed in the vibrational density of states $D(\varepsilon)$ over the energy range of $\varepsilon_0 \leq \varepsilon \leq k_B \Theta_D$, where ε_0 indicates the highest energy of the acoustic phonon branches. The area surrounded by each peak provides three states per unit cell or $3/N$ states per atom. The energy width (full width at half-maximum) of each peak was selected to be $\Delta\varepsilon_{\text{FWHM}} = (k_B \Theta_D - \varepsilon_0) / [b \times (N-1)]$. Although it should have an energy dependence, we set b as a constant value of 5 in the present simulations. The calculated κ_{lat} with $b=5$ provided reasonable results to reproduce κ_{lat} of the 1/1 approximants as shown in the next section. It was also confirmed that a small modification on b does not strongly affect the arguments shown in the next section.

The acoustic phonon branches possess less dispersive portions near the zone boundary, and produces a hump structure

in the vibrational density of states. A small peak of unity in its integrated area was placed at the highest energy of the parabolic portion of the acoustic phonon branches in the same way as the optical phonon peaks, and the parabolic portion in $D(\varepsilon)$ was cut off at a certain energy ε_0 as its area to provide two states per unit cell. We confirmed that the cutoff energy ε_0 thus determined showed a good consistency with the energy where the calculated $D(\varepsilon)$ of the $\text{Al}_{73.6}\text{Re}_{17.4}\text{Si}_9$ deviates from the Debye model. Other minor effects of the zone symmetry were ignored in the calculation of $D(\varepsilon)$.

It is easily understood from Eq. (1) that the parameters required to calculate κ_{lat} are $C(T)$, $v_{\text{ave}}(T)$, and $\lambda(T)$. We calculated these three parameters on the basis of the present phonon model. The lattice specific heat C is calculated from the $D(\varepsilon)$ by simply multiplying the Bose-Einstein distribution function $f_{\text{BE}}(\varepsilon, T)$. To calculate the other factors, the mean group velocity $v_{\text{ave}}(T)$ and the mean free path $\lambda(T)$, we employed a few more assumptions described below.

In contrast with a constant sound velocity v_s , the group velocity of the optical phonon branches v_{opt} varies with momentum and energy, and therefore is hardly estimated. We roughly estimate the group velocity of the optical phonons to be constant as $v_{\text{opt}} = 10 \times (\Delta\varepsilon_{\text{FWHM}}/\varepsilon_0) \times v_s$. The slightly larger prefactor 10 is employed to represent v_{opt} at low energies, because optical phonons at low energies have a stronger influence on κ_{lat} than those at high energies of smaller group velocities. Even with this large prefactor, v_{opt} of the system with $N=138$ is suppressed below $0.1v_s$. The mean group velocity v_{ave} , therefore, is calculated using

$$v_{\text{ave}}(T) = \frac{\int v_s D_a(\varepsilon) f_{\text{BE}}(\varepsilon, T) d\varepsilon + \int b v_s D_o(\varepsilon) f_{\text{BE}}(\varepsilon, T) d\varepsilon}{\int D(\varepsilon) f_{\text{BE}}(\varepsilon, T) d\varepsilon}, \quad (2)$$

where $D_a(\varepsilon)$ and $D_o(\varepsilon)$ indicate partial vibrational density of states associated with the acoustic phonon and the optical phonon, respectively.

In the cubic lattice with lattice constant a , the phonons excited in the volume $A(-G/4 < k_x < G/4, -G/4 < k_y < G/4, -G/4 < k_z < G/4, G=2\pi/a)$ in FBZ hardly contribute to the umklapp scattering process. The probability of the umklapp scatterings, that is reciprocal of the relaxation time τ , increases in proportion to the number of phonons excited outside of the volume A in FBZ. Under this consideration, the partial vibrational density of states directly associated with the umklapp scattering $D_{\text{um}}(\varepsilon)$ is calculated. Although it was possible to employ a slightly different threshold momentum to determine the volume A , the $G/4$ was simply employed because its variation cause a different result only for the system with small lattice constant at low temperatures. In a system with a large lattice constant, which we are very interested in, the shape of $D_{\text{um}}(\varepsilon)$ and the consequently obtained thermal conductivity are not strongly affected by the small variation in the threshold momentum. The relaxation time

associated with the umklapp scatterings is estimated from $D_{\text{um}}(\varepsilon)$ by

$$\tau_{\text{um}}(T) = \left(c \int f_{\text{BE}}(\varepsilon, T) D_{\text{um}}(\varepsilon) d\varepsilon \right)^{-1}, \quad (3)$$

where c represents a factor determining the intensity of the umklapp scatterings.

Other scattering events, such as those by the grain boundary and point defects, were also taken into account with $1/\tau_{\text{gb,pd}} = 1/\tau_{\text{gb}} + 1/\tau_{\text{pd}}$. For the sake of simplicity, we ignore the effects of the complicated electron-phonon scatterings and the minor effects of the normal process³⁰ in the phonon-phonon scatterings. Consequently, the relaxation time for the phonons was estimated by using $\tau(T) = [1/\tau_{\text{um}}(T) + 1/\tau_{\text{gb,pd}}]^{-1}$. Mean free path of the phonons were also calculated by multiplying $\tau(T)$ and $v_{\text{ave}}(T)$. Since phonon scattering associated with grain boundary and the point defects would provide a constant mean free path, the product of $\tau_{\text{gb,pd}}$ and $v_{\text{ave}}(T)$ was treated as constant value λ_{const} in the calculation; $\lambda(T) = \tau v_{\text{ave}}(T) = \{1/[v_{\text{ave}}(T) \cdot \tau_{\text{um}}(T)] + 1/\lambda_{\text{const}}\}^{-1}$.

B. Calculation of lattice thermal conductivity

Now we are ready to discuss the mechanism leading to the small thermal conductivity by calculating the lattice thermal conductivity with Eq. (1) on the basis of the present model. First, we discuss the effects of the large lattice constant a or, in other words, the effects of the large number of atoms N in the unit cell. With increasing a and N , the number of the optical phonon peaks in the $D(\varepsilon)$ increases. Since $D(\varepsilon)$ is calculated for unit volume, the intensity of each peak decreases as a result of the reduced volume of FBZ. Increased number of the peaks in the $D(\varepsilon)$ leads to a drastic reduction in τ_{um} and v_{ave} and a small enhancement of C at low temperature. As a result, κ_{lat} drastically decreases even though other parameters remain unchanged. The calculated $C(T)$, $v_{\text{ave}}(T)$, and $\lambda(T)$ using $\lambda_{\text{const}} = 250 \text{ \AA}$, $c = 2.5 \times 10^{-18} \text{ m}^3 \text{ states}^{-1} \text{ s}^{-1}$ and $\Theta_D = 490 \text{ K}$ are shown in Figs. 6(a1)–6(a3) together with the resulting $\kappa_{\text{lat}}(T)$ in Fig. 6(a4). It is strongly argued, therefore, that the large lattice constant effectively leads to a small thermal conductivity by reducing the group velocity $v_{\text{ave}}(T)$ and by shortening the mean free path with enhancing the probability of the umklapp scatterings.

We discuss the role of vacancies as the second factor. With increasing number of vacancies in the glue sites, the measured $\kappa_{\text{lat}}(T)$ obviously decreases over the whole temperature range while T_{peak} is kept almost unchanged. (see Fig. 2) Since it is natural to imagine that the increased number of vacancies simply reduce the λ_{const} , we calculated the $\kappa_{\text{lat}}(T)$ with some different λ_{const} . The calculated $\kappa_{\text{lat}}(T)$ is shown in Fig. 7(a). The calculated $\kappa_{\text{lat}}(T)$ was indeed decreased with decreasing λ_{const} . However, it occurs only at low temperature, and T_{peak} increases with decreasing λ_{const} . These behaviors are certainly different from the observed ones. Therefore the vacancies do not simply reduce the mean free path but cause some other additional effects.

By increasing the scattering factor c without any variation in other factors, we found that $\kappa_{\text{lat}}(T)$ are drastically de-

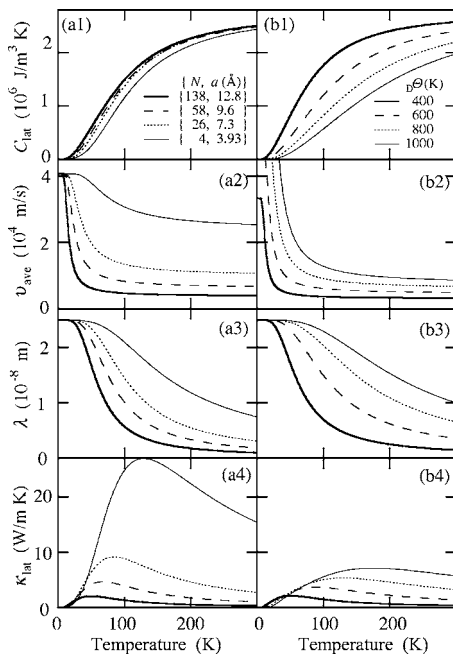


FIG. 6. Simulated specific heat C , mean group velocity v_{ave} , mean free path λ , and the lattice thermal conductivity κ_{lat} . The role of the number of atoms in the unit cell is observable in the panels (a1)–(a4), in which data calculated with four different sets of $(N, a) = (4, 3.93 \text{ \AA})$, $(26, 7.3 \text{ \AA})$, $(58, 9.6 \text{ \AA})$, and $(138, 12.8 \text{ \AA})$ are displayed. Those conditions were determined from fcc (Al), Al_{12}Re , $\text{Al}_5\text{Re}_{24}$, and the $\text{Al}_{73.6}\text{Re}_{17.4}\text{Si}_9$ 1/1-cubic approximant with keeping the density almost constant. The other parameters used in the calculations were $\Theta_D = 490 \text{ K}$, $c = 2.5 \times 10^{-18} \text{ m}^3 \text{ states}^{-1} \text{ s}^{-1}$, and $\lambda_{\text{const}} = 250 \text{ \AA}$. Obviously κ_{lat} drastically decreases with increasing N and a . (b1)–(b4) The variation of specific heat C , mean group velocity v_{ave} , mean free path λ , and lattice thermal conductivity κ_{lat} with varying Θ_D . Four different Debye temperatures, $\Theta_D = 400, 600, 800$, and 1000 K , were employed with $a = 12.8 \text{ \AA}$, $N = 138$, $c = 1.0 \times 10^{-18} \text{ m}^3 \text{ states}^{-1} \text{ s}^{-1}$, and $\lambda_{\text{const}} = 250 \text{ \AA}$. It is clearly understood from the calculated data that the lattice thermal conductivity κ_{lat} decreases with decreasing Θ_D because of the reduction in λ and v_{ave} .

creased over a wide temperature range above T_{peak} as shown in Fig. 7(b). The reduction in $\kappa_{\text{lat}}(300 \text{ K})$ with increasing N_{vac} is seemingly accounted for by this effect. However the peak temperature T_{peak} was decreased by this operation in contrast to the almost constant T_{peak} regardless of the number of the vacancies in the glue sites N_{vac} . Thus the variation in $\kappa_{\text{lat}}(T)$ with N_{vac} cannot be solely accounted for with the increase in the scattering rate c .

Eventually we realized that the vacancies simultaneously cause the reduction in λ_{const} and the enhancement in c . The calculated $\kappa_{\text{lat}}(T)$ with decreasing λ_{const} and increasing c led to the same behavior of $\kappa_{\text{lat}}(T)$ observed when N_{vac} is increased; $\kappa_{\text{lat}}(T)$ decreases at any temperature with T_{peak} kept unchanged [see Fig. 7(c)]. It is strongly pointed out that the introduced vacancies in the approximants have roles not only of reducing the mean free path but also of increasing probability of phonon scatterings.

The presence of vacancies must induce localized motions of their neighboring atoms, such as that in the filled skutteru-

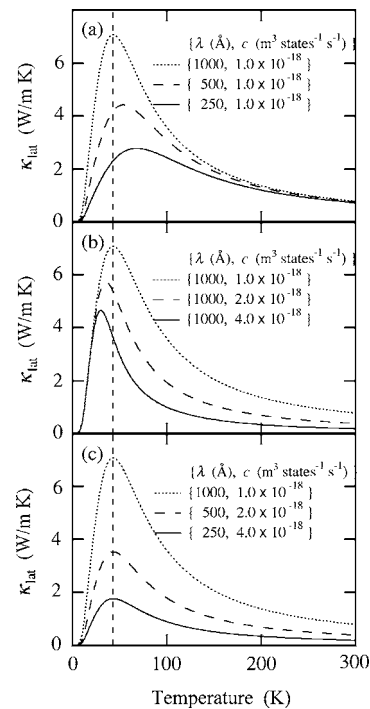


FIG. 7. Variation of the lattice thermal conductivity κ_{lat} with varying (a) the temperature independent mean free path λ_{const} and (b) the scattering parameter c . Variation of κ_{lat} calculated with simultaneously varying λ_{const} and c is shown in (c). The other parameters employed in these calculations were $a = 12.8 \text{ \AA}$, $N = 138$, and $\Theta_D = 490 \text{ K}$. Both reduction in λ_{const} and enhancement in c lead to a significant decrease in the magnitude of the lattice thermal conductivity κ_{lat} . However the peak temperature T_{peak} moves towards opposite temperature side with decreasing λ_{const} and increasing c . The reduction of κ_{lat} with an almost constant T_{peak} observed for the present 1/1-cubic approximants were well accounted for by a reduction in λ_{const} with a simultaneous enhancement in c .

dite structure.³¹ The small thermal conductivity of the skutterudite structure is generally attributed to “the rattling effect” caused by the localized lattice vibration of the weakly bonded, heavy atom. We expect that this rattling effect would be closely related with the vacancy effect that simultaneously causes the enhancement in the probability of phonon-phonon scatterings and reduction in the mean free path.

The role of the heavy constituent elements, such as Re in the $\text{Al}_{82.6-x}\text{Re}_{17.4}\text{Si}_x$ approximants, can be also clearly explained with the present model. The heavier constituent elements naturally lead to a lower Debye temperature Θ_D .²⁵ When a system possesses a smaller Θ_D than other systems of the same crystal structure, all phonon branches are limited in lower energies while the number of the phonon branches is kept unchanged. This condition provides a larger number of optical phonons at a given temperature and, hence, mean group velocity is reduced and umklapp scatterings are enhanced to significantly reduce the mean free path. Considerable reduction in $\lambda(T)$ and $v_{\text{ave}}(T)$ occurs at any temperature, while C is slightly increased at low temperatures as shown in Figs. 6(b1)–6(b3). Consequently, $\kappa_{\text{lat}}(T)$ with a smaller Θ_D possesses a smaller magnitude as shown in Fig. 6(b4).

Since the magnitude of κ_{lat} of the $\text{Al}_{82.6-x}\text{Re}_{17.4}\text{Si}_x$ approximants ($\Theta_D \sim 490 \text{ K}$) (Ref. 12) is less than that of the

$\text{Al}_{82.6-x}\text{Mn}_{17.4}\text{Si}_x$ approximants ($\Theta_D \sim 560$ K),³² the optical phonon branches of the $\text{Al}_{82.6-x}\text{Re}_{17.4}\text{Si}_x$ approximants are expected to stay in the lower energy range than those of the $\text{Al}_{82.6-x}\text{Mn}_{17.4}\text{Si}_x$ approximants. Such a difference in the distribution of phonon branches between the $\text{Al}_{73.6}\text{Re}_{17.4}\text{Si}_9$ and $\text{Al}_{73.6}\text{Mn}_{17.4}\text{Si}_9$ has been already confirmed by our calculation of the phonon dispersion with VASP.³³ The results will be reported elsewhere in the near future.

Variations in strength of the local chemical bonds were sometimes discussed for the icosahedral quasicrystals.^{34,35} It would be worthwhile to mention here that the weaker chemical bonds between the neighboring atoms also lead to lowering of Θ_D and, hence, lowering of κ_{lat} . In order to reveal this effect in much detail, a large amount of calculations is required. Thus, in this paper, we avoid discussing the role of some particular local atomic forces in the approximants.

As a result of the present analysis with the first-principles phonon calculation and the simplified model of phonons, we conclude that the small thermal conductivity of the approximants is mainly brought about by the densely generated optical phonon branches at low energies associated with their large lattice constant and the large number of atoms in the unit cell. The presence of the vacancies in the structure enhances the probability of phonon scatterings and reduces the mean free path of propagating phonons to further reduce the lattice thermal conductivity. The precise, quantitative calculation of $\kappa_{\text{lat}}(T)$ on the basis of the phonon dispersion determined by VASP is now in progress along the method employed in the present study. The result will be reported elsewhere in the near future.

Notably the reduction in the thermal conductivity due to the large N should be of great importance from the engineering point of view. Because this mechanism effectively works without drastically affecting the most crucial factors of the electron scattering, that is the total number of phonons per unit volume. It is predicted from this consideration that artificially produced superlattice structures have a potential to possess an extremely small thermal conductivity without significantly affecting the electrical resistivity, provided that the superlattice periodic ordering is almost perfectly prepared.

Finally we comment on the κ_{lat} of the icosahedral quasicrystals. The Al-based Mackay-type icosahedral quasicrystals have essentially the same behaviors of κ_{lat} with those of the present approximants. The presence of the well-defined

phonons and the pseudo-Brillouin zone (PBZ) were already reported as characteristics of the quasicrystals.^{26–29} Resemblance of the diffraction patterns between quasicrystals and approximants suggests that PBZ in the quasicrystals has the similar shape and size as those of FBZ of the approximants. The umklapp processes over the PBZ, therefore, would frequently take place and effectively reduce κ_{lat} as those in FBZ of the approximants. Although neither presence of the vacancies nor its effect on κ_{lat} has not been revealed for the quasicrystals yet, we strongly expect that vacancies do exist in the structure of some quasicrystals and effectively reduce the κ_{lat} , because large variation in κ_{lat} was also reported for the quasicrystals.^{1–4}

V. CONCLUSION

Thermal conductivity κ of the Al-based Mackay-type 1/1-cubic approximants was investigated in terms of the local atomic arrangements and phonon dispersion. We found that the measured κ of the approximants was not dominated by electrons but by lattice (phonons). Less important role of quasiperiodicity was confirmed from essentially the same behaviors in the lattice thermal conductivity of the approximants and quasicrystals. It was found that κ_{lat} of the approximants possesses small magnitude even with the disordering-free structure and further decreases with increasing vacancies in the glue sites. We conclude, from the first principle phonon calculation and the simulation with a simple phonon dispersion model, that the combination of the small group velocity and the large number of optical phonon branches caused by the large number of atoms in the unit cell effectively reduces κ_{lat} of the approximants by increasing probability of the umklapp process in phonon scattering. Presence of vacancies in the structure further enhance this tendency.

ACKNOWLEDGMENTS

This work was supported by the Grant-in-Aid for Scientific Research for Young Scientists (A) Grant No. 15074207 by the Ministry of Education, Science, and Culture of Japan. The synchrotron radiation experiments were performed at the BL02B2 in SPring-8 with the approval of the Japan Synchrotron Radiation Research Institute (JASRI) (Proposal No. 2004A0262-ND1c-np). The authors (N.N. and R.A.) would like to thank W. Wolf and E. Wimmer in Materials Design Inc., for their useful discussions on phonon calculations.

¹M. A. Chernikov, A. Bianchi, and H. R. Ott, Phys. Rev. B **51**, 153 (1995).

²K. Gianno, A. V. Sologubenko, M. A. Chernikov, H. R. Ott, I. R. Fisher, and P. C. Canfield, Phys. Rev. B **62**, 292 (2000).

³E.-J. Thompson, P. D. Vu, and R. O. Pohl, Phys. Rev. B **62**, 11437 (2000).

⁴A. Bilušić, A. Smontara, J. C. Lasjaunias, J. Ivkov, and Y. Calvayrac, Mater. Sci. Eng., A **294-296**, 711 (2000).

⁵Y. K. Kuo, J. R. Lai, C. H. Huang, C. S. Lue, and S. T. Lin, J. Phys.: Condens. Matter **15**, 7555 (2003).

⁶K. Kirihara and K. Kimura, J. Appl. Phys. **92**, 979 (2002).

⁷A. Pope, T. Tritt, M. Chernikov, and M. Feuerbacher, Appl. Phys.

(N.Y.) **75**, 1854 (1999).

⁸F. S. Pierce, S. J. Poon, and B. D. Biggs, Phys. Rev. Lett. **70**, 3919 (1993).

⁹T. Takeuchi, T. Otagiri, H. Sakagami, T. Kondo, U. Mizutani, and H. Sato, Phys. Rev. B **70**, 144202 (2004).

¹⁰C. Janot, Phys. Rev. B **53**, 181 (1996).

¹¹E. Maciá, Phys. Rev. B **61**, 6645 (2000).

¹²T. Takeuchi, T. Onogi, T. Otagiri, U. Mizutani, H. Sato, K. Kato, and T. Kamiyama, Phys. Rev. B **68**, 184203 (2003).

¹³T. Takeuchi, T. Otagiri, H. Sakagami, T. Kondo, and U. Mizutani, Proceedings of the MRS meeting (Boston, 1 Dec.–5 Dec. 2003), 2004, Vol. 805, pp. 105–110.

- ¹⁴M. Cooper and K. Robinson, *Acta Crystallogr.* **20**, 614 (1966).
- ¹⁵R. Tamura, T. Asao, and S. Takeuchi, *Phys. Rev. Lett.* **86**, 3104 (2001).
- ¹⁶T. Takeuchi, T. Onogi, E. Banno, and U. Mizutani, *Mater. Trans., JIM* **42**, 933 (2001).
- ¹⁷T. Takeuchi and U. Mizutani, *J. Alloys Compd.* **342**, 416 (2001).
- ¹⁸T. Onogi, T. Takeuchi, H. Sato, and U. Mizutani, *J. Alloys Compd.* **342**, 397 (2002).
- ¹⁹F. Izumi and T. Ikeda, *Mater. Sci. Forum* **198**, 321 (2000).
- ²⁰G. Kresse and J. Hafner, *Phys. Rev. B* **47**, 558 (1993); **49**, 14251 (1994).
- ²¹MedeA-Phonon, Materials Design, Inc., 2003, based on K. Parlinski, *Phonon* 3.11, 2002.
- ²²U. Mizutani, T. Takeuchi, and H. Sato, *J. Phys.: Condens. Matter* **14**, R767 (2002).
- ²³R. A. Young, in *The Rietveld Method*, edited by R. A. Young (Oxford University Press, Oxford, 1993), Chap. 1.
- ²⁴K. Edagawa and K. Kajiyama, *Mater. Sci. Eng., A* **294-296**, 646 (2000).
- ²⁵For example, J. M. Ziman, *Electrons and Phonons* (Oxford University Press, Oxford, 1960).
- ²⁶M. de Boissieu, M. Boudard, H. Moudden, M. Quilichini, R. Bellisent, B. Hennion, R. Currat, A. Goldman, and C. Janot, *J. Non-Cryst. Solids* **153&154**, 552 (1993).
- ²⁷M. de Boissieu, R. Currat, S. Franconal, and E. Kats, *Phys. Rev. B* **69**, 054205 (2004).
- ²⁸S. Francoual, K. Shibata, M. de Boissieu, A. Q. R. Baron, S. Tsutsui, R. Currat, H. Takakura, A. P. Tsai, T. Lograsso, and A. R. Ross, *Ferroelectrics* **305**, 209 (2004).
- ²⁹M. Windisch, J. Hafner, M. Krajčí, and M. Mihalkovič, *Phys. Rev. B* **49**, 8701 (1994).
- ³⁰J. Callaway, *Phys. Rev.* **113**, 1046 (1959).
- ³¹B. C. Sales, D. Mandrus, B. C. Chakoumakos, V. Keppens, and J. R. Thompson, *Phys. Rev. B* **56**, 15081 (1997).
- ³²T. Takeuchi, *Philos. Mag.* **86**, 1037 (2006).
- ³³N. Nagasako, R. Asahi, and T. Takeuchi (unpublished).
- ³⁴T. Nagata, K. Kirihara, and K. Kimura, *J. Appl. Phys.* **94**, 6560 (2003).
- ³⁵K. Kirihara, T. Nakata, M. Takata, Y. Kubota, E. Nishibori, K. Kimura, and M. Sakata, *Phys. Rev. Lett.* **85**, 3468 (2000).